Measurement of Exciton Transport in Conjugated Polymer Nanoparticles

Louis C. Groff[†], Xiaoli Wang[†], and Jason D. McNeill*[†]

[†]Department of Chemistry, Clemson University, Clemson, SC, USA 29634

Corresponding Author, *E-mail: mcneill@clemson.edu

ABSTRACT

A novel approach is proposed for determining exciton transport parameters in conjugated polymers. Exciton dynamics of conjugated polymer nanoparticles doped with dyes were investigated by time-resolved fluorescence spectroscopy. Highly efficient energy transfer from the polymer PFBT to the dye perylene red was evident in the fluorescence spectra and excited state kinetics. Exciton transport parameters were obtained by fitting to a model that included the effects of nanoparticle size, exciton diffusion, energy transfer, and quenching by defects. The results indicate substantial quenching by defects, owing primarily to exciton diffusion, which can greatly increase the effective quenching volume of defects. We estimated the amount of quenching by defects, and included quenching by defects in our model, yielding an estimated exciton diffusion length of 12 nm and diffusion constant of 8.0×10^{-9} m^2 s^{-1} for nanoparticles of PFBT. The results indicate that quenching by defects can lead to substantial error in determined exciton transport parameters, unless such quenching is properly accounted for in the model.

KEYWORDS

Diffusion, Energy Transfer, Organic Semiconductors, Quenching, Modeling

INTRODUCTION

In recent years, there has been a great deal of interest in conjugated polymers, largely due to their application as the active materials in flexible, low-cost, highly efficient photovoltaic[1] and light-emitting devices.[2] Conjugated polymer nanoparticles (CPNs) are of interest for use in biological imaging, given their high fluorescence brightness, extraordinary two-photon fluorescence cross-sections, and excellent photostability.[3-9] It is increasingly clear that further development of applications requires additional understanding of the complex photophysics and photochemistry of conjugated polymers, as well as their dependence on polymer structure and processing conditions. In organic semiconductors, the principal neutral electronic excitation of interest is typically the Frenkel-type singlet exciton.[10,11] Energy transfer between sites or chromophores occurs via multiple processes, including incoherent, diffusion-like processes,[12-14] dispersive transport,[15] and in some cases, via ultrafast, long range coherent transport.[16] In the exciton diffusion picture, each polymer chain is considered to consist of several more or less independent chromophores or exciton sites, and excitations transfer from one site to other nearby sites via transition dipole-mediated Förster transfer.[17] Multiple excitation transfer events typically occur during the excited state lifetime, resulting in a random walk-like process characterized by a diffusion constant or length. A large exciton diffusion length is required for optimum photovoltaic device efficiency (for some device types), since excitons must travel to the heterojunction to undergo charge separation. While the exciton diffusion length in high purity, crystalline inorganic semiconductors can reach several microns,[18] it is typically much shorter for organic semiconductors. For example, measured exciton diffusion lengths for single crystals of

anthracene range from ~30 nm to 60 nm,[19-21] and diffusion lengths of under 15 nm are typically reported for conjugated polymers.[22-24] Interacting chromophores can also give rise to aggregate species such as dimers, H- and J-aggregates, excimers, and exciplexes.[25,26] Energy transfer can also occur to these and other species such as excess charges (polarons),[27] defects introduced during polymer synthesis or processing,[28] or dopant species such as dyes and other polymers.[23,29] These processes can significantly reduce the observed exciton diffusion length. Various experimental methods have been developed for characterizing exciton diffusion, including photoluminescence quenching in layered structures,[12,30] confocal fluorescence microscopy,[31] near-field fluorescence microscopy,[32-34] time-resolved fluorescence of dye-doped films, crystals, or nanoparticles,[14,22,23,35] and single particle imaging.[36,37] Different assumptions are involved in the various methods, each contributing to different types of systematic error or bias, leading to a wide range of reported exciton diffusion lengths, as discussed by Forrest *et al*.[12]

Here, we examine some processes relevant to the determination of exciton diffusion constants in dye-doped conjugated polymer nanoparticles by way of time-resolved fluorescence spectroscopy. In particular, we examine the effects of quenching by defects on the observed quenching efficiencies and excited state dynamics. While quenching by defects[28] and hole polarons[37] has been observed, quenching by defects is rarely quantified in studies of exciton transport dynamics in conjugated polymers, perhaps since it is preferable to minimize defects by employing proper technique. However, in some cases defects can be difficult to avoid entirely, or there may be quenching by intrinsic species such as aggregates, exciplexes, or photogenerated polarons. Furthermore, the combination of energy transfer and exciton diffusion can result in quenching radii as large as 10 nm.[38] Thus, even very low concentrations of defects or other quenching species could give rise to significant quenching. Additionally, quenching by hole

polarons is significant at a polaron density of $5x10^{17}$ cm^{-3},[27,39] which is often exceeded in functioning devices. We observe complex fluorescence decay dynamics consistent with significant quenching by defects in undoped nanoparticles of MEH-PPV and PFBT. Therefore, we develop a modified approach to determining exciton diffusion parameters that explicitly includes quenching by defects. By fitting the quenching efficiencies and complex fluorescence decay kinetics to an exciton diffusion model that explicitly includes quenching by defects, we obtain a corrected exciton diffusion length for nanoparticles of the polymer PFBT. Our results indicate typical analysis ignoring defects results in underestimation of L_D by roughly a factor of 2. Analysis of the distribution of lifetimes provided additional confirmation of quenching by defects: The fluorescence decays of doped and undoped particles were fit to a stretched exponential function, yielding a stretch parameter *ß*, which typically varies between ~0.3, indicating a broad distribution of lifetimes, and ~1.0, indicating a very narrow distribution (a single lifetime). Fitting the dynamics of undoped particles yielded *ß* = 0.6, consistent with significant quenching by defects. Analysis of the radiative and non-radiative rates was also consistent with quenching by defects. Our results indicate that quenching by defects can lead to significant underestimation of the exciton diffusion length, particularly for highly mobile excitons, which are highly susceptible to quenching, even at very low densities of quenching species or defects. The results are also promising for applications requiring highly mobile excitons, such as photovoltaic devices, since improvements in exciton diffusion length by a factor of 2 or more are expected if quenching by defects can be substantially reduced.

EXPERIMENTAL METHODS

Materials. The copolymer poly[(9,9-dioctylfluorenyl-2,7-diyl)-*co*-(1,4-benzo-{2,1',3}-thiadiazole)] (PFBT, MW 10,000, polydispersity 1.7) was purchased from ADS Dyes, Inc.

(Quebec, Canada). The fluorescent dye perylene red (Exalite 613) was purchased from Exciton (Dayton, OH). The fluorescent dye fluorescein was purchased from Invitrogen (Eugene, OR). The solvent tetrahydrofuran (THF, anhydrous, inhibitor-free, 99.9%) and sodium hydroxide (SigmaUltra, minimum 98%) were purchased from Sigma-Aldrich (Milwaukee, WI). All chemicals were used as provided without further purification.

Nanoparticle Preparation. Preparation of the fluorescent nanoparticles was performed using a previously described nano-precipitation method.[40] The copolymer PFBT was dissolved in THF by gentle agitation and prepared at a concentration of 1000 ppm. Perylene red was dissolved in THF by gentle agitation and prepared at a concentration of 100 ppm. The solution was further diluted to 2 ppm for mixing with the polymer solution. Varying amounts of the dopant perylene red solution were mixed with the PFBT solution to produce solution mixtures with a concentration of 20 ppm PFBT and dopant/host fractions of 0 to 2 wt% perylene red. The mixtures were sonicated very briefly to ensure homogeneity. A 2 mL quantity of each solution mixture was added rapidly to 8 mL of deionized water under sonication for ~30 s at a sonication frequency of 40 kHz and room temperature. THF was removed from the resulting nanoparticle suspensions by partial vacuum evaporation and subsequently vacuum filtered through a glass fiber prefilter to remove larger aggregates and a 0.1 μm PVDF membrane filter. The resulting nanoparticle suspensions are clear (not turbid) and stable for months with no visible signs of aggregation.

Characterization Methods. Size distributions and morphologies of undoped and perylene red doped PFBT nanoparticles were determined by atomic force microscopy (AFM). Samples were prepared by dipcasting a freshly cleaned glass coverslip in a diluted nanoparticle suspension for 40 minutes, then removing the coverslip and allowing it to dry overnight in an

enclosed environment. Surface topographies were measured on an Ambios Q250 multimode AFM in AC mode. The particle diameters were obtained from height analysis.

UV-Vis absorption spectra were collected on a Shimadzu UV2101PC scanning spectrophotometer using 1 cm quartz cuvettes. Fluorescence spectra were collected and fluorescence quantum yield was measured using a commercial fluorimeter (Quantamaster, Photon Technology International, Inc.) using 1 cm quartz cuvettes. Fluorescein in 0.01 M sodium hydroxide was utilized as a standard to determine the fluorescence quantum yield of the PFBT CPN samples. 473 nm was selected as the excitation wavelength. A Förster radius of 3 nm for the PFBT/perylene red donor/acceptor pair was calculated utilizing the absorption spectrum of perylene red in THF and the emission spectrum of undoped PFBT CPNs using standard methods,[41] correcting for the polymer refractive index and assuming an orientation factor of $\kappa^2 = 2/3$, which is the standard result for dynamic reorientation of transition dipoles.

Fluorescence lifetimes were measured in air using time-correlated single photon counting (TCSPC) spectroscopy. The second harmonic (420 nm) of the output of a mode-locked Ti:Sapphire laser (Coherent Mira 9000, 840 nm, ~150 fs pulsewidth) was used to excite the sample. The output of a fast PIN diode (Thorlabs DET210) was used as the start pulse for a time-to-amplitude converter (TAC, Canberra Model 2145). Nanoparticle fluorescence was collected perpendicular to the excitation source after passing through a 460 nm long pass filter for the undoped nanoparticles. An additional 540 ±10 nm band pass filter was added for the doped samples in order to filter out the emission from perylene red. The emission was detected by a single photon avalanche photodiode (id Quantique, id100-50). The output of the APD was used as the stop pulse for the TAC. The excitation pulse was attenuated to maintain a count rate of ~6 kHz. The analog signal from the TAC was digitized using a multichannel analyzer (FastComTec,

MCA-3A). Before and after each fluorescence lifetime measurement, the instrument response function (IRF) was measured using scattered laser light from a dilute suspension of polystyrene microspheres. The width of the resulting IRF was determined to be ~80 ps (FWHM).

RESULTS/DISCUSSION

Initial characterization of dye-doped PFBT CPNs. Doping of conjugated polymer nanoparticles (CPNs) with dyes is being pursued as a strategy for improving their brightness and photostability while red-shifting their fluorescence, and as a way to investigate exciton diffusion in conjugated polymers. PFBT was selected as the host polymer owing to its excellent photostability and high fluorescence quantum yield, as well as its broad fluorescence spectrum, which facilitates energy transfer to dyes.[6] Perylene red was selected as the dye dopant for this system due to the excellent spectral overlap with the emission spectrum of PFBT and its high fluorescence quantum yield (0.96 in chloroform).[42,43] Perylene red-doped PFBT CPNs were prepared via a nano-precipitation method described previously.[40] Samples were filtered through a 0.1 μm membrane filter and characterized via UV-Vis and fluorescence spectroscopy. Size distributions were determined via particle height analysis of representative AFM images (c.f. Fig 1). The AFM images are consistent with spherical nanoparticles, as is expected for glassy polymers in this size range, based on surface free energy considerations. Terentjev et al. previously reported spherical morphology for particles of PFBT roughly in this size range.[44]

Energy transfer efficiency as high as 86% was observed at 2% doping, where the energy transfer efficiency is given by $\eta_{ET} = 1 - F/F_0$, and F, F_0 are the host fluorescence intensity in the presence, absence of dopant, respectively (c.f. Fig 2). It was expected that most of the dye is incorporated into the nanoparticles owing to the hydrophobic character of the dye, based on previous results examining incorporation of dyes with similar solubility properties, using

centrifugal concentration to examine dye incorporation and possible leaching.[23] Additionally, the lack of additional features in the UV-vis and fluorescence spectra that could be ascribed to free dye or dye aggregate in solution is evidence that the fraction of unincorporated dye is small (less than a few percent). Finally, the high energy transfer efficiency at low doping ratios provides additional confirmation that a high fraction of the dye molecules are incorporated in the nanoparticles. The intensity of acceptor emission in the doped samples increases as dopant is added up to 0.5% doping. Upon further doping, acceptor emission intensity decreases. We ascribe this to aggregation quenching of the acceptor as dye dimers form within the nanoparticle at higher doping levels. Aggregate formation could also explain the red shift of the acceptor emission observed at higher doping levels. Stern-Volmer analysis was performed using the quencher/donor molecular fraction $f = n_{dye}/n_{poly}$ as the unit of concentration, in order to obtain K_{SV} in terms of the number of polymer molecules quenched per perylene red molecule. The analysis yields a quenching constant of 37 per dye molecule, indicating that roughly 37 PFBT molecules are quenched per dye molecule. From this result, an effective dye quenching radius of 5.3 nm is obtained, which is significantly larger than the calculated Förster radius, providing initial indication of exciton diffusion.

The quantum yield of undoped PFBT CPNs was measured to be 0.14, consistent with prior measurements.[6,45,46] The total fluorescence quantum yield of the doped samples decreases monotonically with increasing dopant concentration, indicating that doping with this dye does not increase CPN brightness as initially hoped (c.f. Fig 2). However, at moderate doping levels (0.5%-1%), the decrease in fluorescence quantum yield is minimal, while the energy transfer efficiency is high, thus doping with perylene red can be used to red-shift the fluorescence while maintaining high levels of brightness. In microscopic imaging experiments, signal levels and

contrast are affected by several phenomena and factors related to the spectroscopy of the dyes and the experimental setup.[47] A key issue is autofluorescence from the sample and from the various optical materials. Autofluorescence typically peaks a few nm to the red of the excitation wavelength, with a long red tail. Thus, for typical dyes with small Stokes shifts, selection of filters involves a compromise between efficient collection of the emission of interest and rejection of autofluorescence. The PFBT nanoparticles doped with perylene red exhibit a large red-shift in the emission, which is advantageous for efficient collection of fluorescence and rejection of autofluorescence.

Picosecond time-resolved fluorescence spectroscopy. Time-correlated single photon counting (TCSPC) was employed to determine the lifetimes of the excited state in doped and undoped nanoparticles of PFBT, and for the polymer dissolved in THF. The decay trace was fit by a least-squares minimization procedure involving convolution of a trial decay function with the instrument response function. The trial functions are (single) exponential, bi-exponential, and the stretched exponential or Kohlrausch-Williams-Watts (KWW) function,

$$F(t) = Ae^{-(t/\tau)^{\beta}} \quad (1)$$

The stretch-parameter ß acts as a measure of lifetime heterogeneity, ranging between ~0.3 and 1, where lower values indicate a broad distribution of lifetimes while ß = 1 corresponds to a single lifetime.[48] The fluorescence decay of PFBT in THF was adequately fit by a single exponential, while the decays of undoped nanoparticles and lightly to moderately-doped particles (0.1%-1.0%) exhibited complex decay kinetics that fit well to both bi-exponential and stretched exponential (KWW) functions. While single exponential fits converged for all samples, bi-exponential and KWW fits did not converge for 1.5% and 2% doping due to low signal levels and short lifetimes relative to the width of the instrument response function. Results show a clear

decreasing trend in lifetimes as the doping ratio is increased, with perhaps a slight decreasing trend in ß (c.f. Fig 3), though it is not clear that the decrease is statistically significant. In any case, the ß values indicate a broad distribution of exciton lifetimes for the nanoparticles, consistent with energy transfer in dense multichromophoric systems,[23] while the polymer in THF yielded ß values near unity, suggesting little energy transfer. Overall, the weighted average lifetimes and ß values obtained from the fits are consistent with the physical picture of exciton diffusion and energy transfer, i.e., dynamic quenching due to energy transfer, which will be discussed in more detail below.

Modeling exciton diffusion and energy transfer. Exciton dynamics in doped conjugated polymers can be described as mobile excitons hopping from site to site in a random, diffusion-like process prior to decaying (both radiatively and non-radiatively) or undergoing energy transfer to a defect or dopant molecule.[49-51] In this picture, a key exciton transport parameter is the diffusion length, $L_D = \sqrt{2nD\tau}$, where n is the dimensionality, D is the (1D) diffusion constant, and τ is the exciton lifetime. We previously developed a numerical random walk approach to modeling the combined effects of exciton diffusion and energy transfer in CPNs, which yielded values for energy transfer efficiency that were in agreement with experimental results for dye-doped CPNs.[23] This approach was also applied to modeling fluctuations in the fluorescence centroid of a single CPN due to polaron motion.[37] Here, we have modified the previous simulation code to provide kinetics information for comparison to the time-resolved fluorescence results. We have also modified our approach to explicitly account for quenching by defects. Neither coherent transport nor dispersive transport are explicitly included in the present approach.[15,16] The simulation algorithm is described briefly as follows (additional simulation details are provided in the Supporting Information). Dopant dyes and/or defects are

distributed randomly within the nanoparticle, represented by a sphere. While a sphere is assumed, similar results are obtained assuming a cubic particle.[36,37] Here we define "defects" as any of a number of quenching species such as polarons, aggregate species, conformational defects, oxidized defects and synthetic defects, which are not deliberately introduced into the system, in contrast to the dye molecules, which are deliberately added in controlled amounts. In these simulations, dopant dyes are essentially treated as points within a continuum. However, the model may be adjusted to correct for finite dye volume effects (e.g. by adjusting the Förster radius). An initial population of excitons is also distributed randomly within the sphere. For each time step Δt, each exciton is propagated by adding to its position along each axis a Gaussian-distributed random number scaled so that $\sigma^2=2D\Delta t$, where D is the (1D) diffusion constant and σ^2 is the variance of the random number distribution (μ = 0). Then the energy transfer rate for each exciton to each dopant or defect is calculated based on the exciton-acceptor distances and the conventional Förster rate expression. Based on the rates of energy transfer, radiative decay, and non-radiative decay, the probability of decay or transfer for a given exciton during the time step is calculated and compared to a random number to determine the exciton fate. The exciton population is updated accordingly, and recorded for each time step. The simulation continues until nearly all of the exciton population has decayed. The simulations are performed for many initial random configurations of acceptors and excitons, and the exciton population kinetics and energy transfer efficiencies are calculated from the simulation results.

We explicitly include exciton quenching by defects (which can include aggregates, polarons, excimers, synthetic defects, oxidized defects, etc.) as a key feature in our approach to modeling exciton diffusion and energy transfer in the nanoparticles. The explicit inclusion of quenching by defects is based on several observations. First, the fluorescence quantum yield and

excited state lifetime of the nanoparticles is greatly reduced (Φ = 0.14, τ_{avg} = 800 ps) as compared to the polymer in a good solvent such as THF (Φ = 0.66, τ_{avg} = 3000 ps). The phenomenon of reduced lifetimes in the aggregated state is often observed in J-aggregates, and is typically described as due to coupling of the transition dipole moments that causes a large increase in the radiative rate.[52] However, strong J-aggregate-type coupling is not likely to be responsible for the decrease in lifetime in the present case, since little shift in the absorption spectrum is observed upon nanoparticle formation (c.f. Fig. S1 in Supporting Information), indicating weak coupling. Furthermore, the radiative rate, estimated from the lifetime and quantum yield values, is actually somewhat lower in the nanoparticles (1.8×10^8 s^{-1}), as compared to the polymer in THF (2.2×10^8 s^{-1}), which does not correspond to typical J-aggregate behavior. Finally, the heterogeneity of the excited state lifetime of the nanoparticle is increased ($ß$ = 0.65) as compared to the free polymer in solution ($ß$ = 1.0), consistent with quenching by energy transfer to some type of defect species, which could include oxidized defects, synthetic defects, aggregate species, exciplexes, and/or hole polarons (cations). Evidence for the existence of photogenerated hole polarons in PFBT CPNs is given in previously published work.[37] Additional support for the hypothesis of dynamic quenching by defects is given by analysis of the excited state lifetime and quantum yield results, which are not consistent with static quenching. Finally, the defect-quenching hypothesis is also supported by the agreement between experimental results and the exciton diffusion-energy transfer simulations, discussed below.

In order to account for quenching by defects in the simulation, the defect density (expressed as dye equivalents per nanoparticle) has been added as a model parameter. Exciton diffusion simulations were carried out for a particle of radius 4 nm, to match the 8 nm diameter determined by AFM (c.f. Fig. 1), with the exciton diffusion length set at 12 nm, and the time step

set to 1 ps. In order to simulate a given dye and/or defect density, first the Poisson distribution of dyes or defects per nanoparticle was calculated based on the average number of dyes or defects per nanoparticle, (e.g., if there are 1.7 dyes per particle on average, the Poisson distribution is used to estimate what population fraction of particles has 0, 1, 2, or 3 dyes, and so on) and simulations were performed assuming various numbers of dyes per nanoparticle. Then the kinetics curves and energy transfer efficiencies were combined using Poisson statistics to produce a weighted average kinetics curve and energy transfer efficiency for the dopant density of interest. Initially, a Förster radius of 3 nm was calculated from the spectra of perylene red and PFBT in THF using standard methods and assuming a value of 2/3 for the orientation factor κ^2.[41] However, while the match to experimental lifetimes and *ß* values improved, the simulation results did not match experimental quenching efficiencies well. It is likely that local ordering of the polymer could result in a somewhat larger value of the orientation factor, or that other physical processes such as coherent transport could lead to a larger quenching radius.[15,16] Thus, simulations were carried out using an increased R_0 of 4 nm. This improved the agreement with experimental quenching efficiencies.

The defect density was estimated by comparison of simulation results to experimental results as follows. It was assumed that quenching by defects occurs primarily via a combination of exciton diffusion and energy transfer, and thus quenching is greatly reduced for the polymer in good solvent, since exciton diffusion is essentially eliminated and energy transfer is greatly reduced when the polymer adopts an open conformation (due to the increased inter-chromophore distance), while the polymer in the collapsed, aggregated state possesses a relatively higher chromophore density, favoring both energy transfer and exciton diffusion. Indeed, prior work shows that even a single defect or dopant per CPN can result in substantial quenching.[23,37] The

assumption of relatively little quenching for the polymer in an open, unaggregated conformation is supported by the much higher fluorescence quantum yield and single-exponential decay kinetics observed for the polymer dissolved in THF (decay kinetics are typically complex when energy transfer over a range of distances occurs). Thus a comparison between the fluorescence quantum yield and kinetics for the polymer dissolved in good solvent versus for the polymer in the nanoparticle state yields information about the extent of quenching in the nanoparticle. A defect quenching efficiency of 0.79 was estimated, based on a comparison of the quantum yields of the dissolved polymer and the CPNs. To estimate the defect density, we performed exciton diffusion and energy transfer simulations as described above, using the lifetime of the polymer in good solvent and assuming the same Förster radius as the dye and the same L_D parameter used to model the dye-doped CPNs. The defect density was varied until good agreement with the experimental average lifetime, β parameter, and fluorescence quantum yield of the undoped CPN's was obtained. The defect density corresponding to the best fit for the undoped nanoparticles varied depending on the L_D parameter, but for L_D = 12, (the global best-fit value, see below) an effective defect density of 2.3 dye equivalents per 8 nm dia. nanoparticle was obtained.

To further test the model and assumptions, and to obtain the exciton diffusion length, simulations were also performed including doping with the perylene red dye, varying the exciton diffusion length to provide the best match to experimental quenching efficiencies and exciton decay kinetics. Based on the weight fraction of the dye, the average number of dyes per nanoparticle was calculated, and this was added to the number of defects determined previously. The quenching efficiencies and fluorescence decays obtained from the simulation are compared to experimental results in Fig. 4, for L_D = 12 nm, with the density of dye represented as a ratio of

the number of dyes to the number of polymer molecules (given the molecular weights of the polymer and dye, a molecular ratio of 0.10 corresponds to a weight fraction of 1.0% or a dye density of $6x10^{18}$ dyes per cubic centimeter of polymer). By utilizing the lifetime and quenching efficiency results for the nanoparticles at various doping levels as well as for the polymer in good solvent, we are able to probe the relative contributions of exciton diffusion, energy transfer, and quenching by defects on the exciton diffusion length. In introducing the Poisson distribution of defects and dyes, there is a trade-off in that the match with the experimental quenching efficiencies is somewhat poorer, but the match to the lifetimes and particularly the KWW stretch parameter is greatly improved, as compared to the results of simulations that neglected Poisson statistics and quenching by defects (simulation results provided in the Supporting Information). Nevertheless, the simulation results obtained including the Poisson distribution for defects and dyes fit reasonably well to all of the experimental results. The obtained exciton diffusion length of 12 nm is similar to that obtained for polyfluorene films by a different method.[22]

The Stern-Volmer analysis yields a quenching radius of 5.3 nm for perylene red--significantly higher than the Förster radius R_0, even if we make favorable assumptions regarding orientation, clearly indicating that exciton diffusion contributes significantly to the quenching efficiency of the dye. However, analysis of the quenching efficiencies alone does not clearly indicate the relative contributions of L_D and R_0: Results of exciton diffusion simulations (given in the Supporting Information) indicate that an increase in *either* L_D or R_0 (or both) results in an increase in quenching efficiency. While there is no simple, exact analytical formula relating L_D and R_0 to the β parameter, we found that β increases monotonically with increasing L_D, (i.e., increasing L_D results in a decrease in the amount of heterogeneity in energy transfer rates) while β decreases as R_0 increases. By including analysis of the β parameter, as well as quenching by

defects, we obtained a significantly larger value for the Förster radius than that obtained using the typical assumption of $\kappa^2 = 2/3$, suggesting that this assumption may not be accurate for this system.[23] These results strongly suggest that a combined approach of measuring exciton decay kinetics, quenching efficiency, and modeling (in which quenching by defects is explicitly included) is necessary in order to disentangle the combined effects of exciton diffusion and energy transfer on exciton quenching efficiencies and dynamics.

Another important issue is the effect of quenching by defects on the determined exciton diffusion parameters, particularly the diffusion length and calculated R_0. By explicitly including quenching by defects in the simulation and analysis, we obtain an (intrinsic) exciton diffusion length (i.e., an exciton diffusion length for a hypothetical defect-free material). The intrinsic exciton diffusion length is 85% larger than the phenomenological diffusion length obtained from dye-quenching analysis without inclusion of defect quenching. This result has several implications. First, that for cases where conjugated polymers exhibit a large decrease in fluorescence quantum yield in the aggregated state (i.e., films and particles) relative to the polymer dissolved in a good solvent, this may indicate highly mobile excitons undergoing energy transfer to a small fraction of defects. Thus, somewhat paradoxically, a large value of D can result in a small observed value for the diffusion length, *which in many such cases is determined largely by the density of quenching defects rather than by the diffusion constant*. Second, the approach and results presented here suggest a general method for determining both the defect density and the effect of quenching by defects on the measured exciton diffusion length. Third, the low defect densities we obtained (much lower than 1 defect per polymer chain) and large exciton diffusion lengths determined in the absence of quenching lend qualitative support to the extraordinarily large exciton diffusion lengths reported in the single molecule studies of Barbara

et al.[36] Additionally, the significantly larger exciton diffusion length obtained from the lifetime analysis is promising for applications requiring large exciton diffusion lengths, such as photovoltaic devices. Finally, while the nature of quenching defects varies from polymer to polymer, in the case of some PPV derivatives as well as polyfluorene derivatives, quenching defects appear to be partially oxidized polymer, or hole polarons.[28,46] In the case of hole polarons, quenching by defects can sometimes be suppressed by addition of electron-donor species.[46] Thus the addition of such species could be helpful for applications requiring larger exciton diffusion lengths.

CONCLUSIONS

PFBT CPNs doped with perylene red dye were found to exhibit efficient energy transfer from the polymer host to the dye. The excited state dynamics of the dye doped CPNs were studied by steady state and time-resolved fluorescence methods. The spectra are red-shifted significantly with only minor losses in fluorescence quantum yield, indicating that these nanoparticles provide bright, red emission, which is useful for some imaging and tracking applications. The lifetime of the donor exciton is reduced and the width of the distribution of exciton lifetimes was found to increase as the dopant concentration increases, as determined by time-resolved fluorescence. We interpret the kinetics results and the results of simulations as indicating substantial quenching by defects, which is amplified by exciton diffusion. The simulation parameters were adjusted until a reasonably good fit was obtained to the experimental results, including the quenching efficiency results, the average lifetimes, and the KWW stretch parameter. Based on the fitting results, an exciton diffusion length of 12 nm for PFBT CPNs was obtained, corresponding to a diffusion constant of 8.0×10^{-9} m^2 s^{-1}. The results provide some indication that quenching by defects or other quencher species is a significant but often

overlooked issue in aggregated conjugated polymers, and the approach described here--combining steady-state and time-resolved spectra of the dissolved polymer and doped nanoparticles--is proposed as a more or less general method for quantifying both exciton transport and exciton quenching by defects in conjugated polymer materials. Additionally, our analysis suggests that for some conventional approaches to determining exciton diffusion lengths, the result may be largely determined by the defect density.

ACKNOWLEDGMENT

We acknowledge financial support from the NSF under Grant No. CHE-1058885.

SUPPORTING INFORMATION

Detailed procedures of conjugated polymer nanoparticle preparation and characterization, fluorescence quantum yield, picosecond fluorescence lifetime measurements, and exciton modeling details are supplied as Supporting Information. This material is available free of charge via the Internet at http://pubs.acs.org.

REFERENCES

(1) Dennler, G., and Sariciftci, N. S. Flexible Conjugated Polymer-Based Plastic Solar Cells: From Basics to Applications. *Proc. IEEE* **2005**, *93*, 1429-1439.

(2) Yim, K. H., Zheng, Z., Liang, Z., Friend, R. H., Huck, W. T. S., and Kim, J. S. Efficient Conjugated-Polymer Optoelectronic Devices Fabricated by Thin-Film Transfer-Printing Technique. *Adv. Funct. Mater.* **2008**, *18*, 1012-1019.

(3) Wu, C. F.; Szymanski, C.; Cain, Z.; McNeill, J. Conjugated Polymer Dots for Multiphoton Fluorescence Imaging. *J. Am. Chem. Soc.* **2007**, *129*, 12904-12905.

(4) Yu, J., Wu, C. F., Sahu, S. P., Fernando, L. P., Szymanski, C., and McNeill, J. Nanoscale 3D Tracking with Conjugated Polymer Nanoparticles. *J. Am. Chem. Soc.* **2009**, *131*, 18410-18414.

(5) Wu, C. F., Bull, B. Christensen, K. and McNeill, J. Ratiometric Single-Nanoparticle Oxygen Sensors for Biological Imaging. *Angew. Chem., Int. Ed.* **2009**, *48*, 2741-2745.

(6) Wu, C. F.; Bull, B.; Szymanski, C.; Christensen, K.; McNeill, J. Multicolor Conjugated Polymer Dots for Biological Fluorescence Imaging. *ACS Nano* **2008**, *2*, 2415-2423.

(7) Wu, C. F.; Schneider, T.; Zeigler, M.; Yu, J. B.; Schiro, P. G.; Burnham, D. R.; McNeill, J. D.; Chiu, D. T. Bioconjugation of Ultrabright Semiconducting Polymer Dots for Specific Cellular Targeting. *J. Am. Chem. Soc.* **2010**, *132*, 15410-15417.

(8) Wu, C. F.; Chiu, D. T. Highly Fluorescent Semiconducting Polymer Dots for Biology and Medicine. *Angew. Chem., Int. Ed.* **2013**, *52*, 3086-3109.

(9) Koner, A. L.; Krndija, D.; Hou, Q.; Sherratt, D. J.; Howarth, M. Hydroxy-Terminated Conjugated Polymer Nanoparticles Have Near-Unity Bright Fraction and Reveal Cholesterol-Dependence of IGF1R Nanodomains. *ACS Nano* **2013**, *7*, 1137-1144.

(10) Emelianova, E. V., Athanasopoulos, S., Silbey, R. J., and Beljonne, D. 2D Excitons as Primary Energy Carriers in Organic Crystals: The Case of Oligoacenes. *Phys. Rev. Lett.* **2010**, *104*, 206405-206408.

(11) Kasha, M.; Rawls, H. R.; El-Bayoumi, M. A. The Exciton Model in Molecular Spectroscopy. *Pure Appl. Chem.* **1965**, *11*, 371-392.

(12) Lunt, R. R., Giebink, N. C., Belak, A. A., Benzinger, J. B., and Forrest, S. R. Exciton Diffusion Lengths of Organic Semiconductor Thin Films Measured by Spectrally Resolved Photoluminescence Quenching. *J. Appl. Phys.* **2009**, *105*, 053711-053717.

(13) Gammill, L. S.; Powell, R. C. Energy-Transfer in Perylene Doped Anthracene-Crystals. *Mol. Cryst. Liq. Cryst.* **1974**, *25*, 123-130.

(14) Powell, R. C.; Kepler, R. G. Evidence for Long-Range Exciton-Impurity Interaction in Tetracene-Doped Anthracene Crystals. *Phys. Rev. Lett.* **1969**, *22*, 636-639.

(15) Athanasopoulos, S.; Hoffman, S. T.; Bassler, H.; Kohler, A.; Beljonne, D. To Hop or Not to Hop? Understanding the Temperature Dependence of Spectral Diffusion in Organic Semiconductors. *J. Phys. Chem. Lett.* **2013**, *4*, 1694-1700.

(16) Scholes, G. D., and Rumbles, G. Excitons in Nanoscale Systems. *Nat. Mater.* **2006**, *5*, 683-696.

(17) Burkalov, V. M., Kawata, K., Assender, H. E., Briggs, G. A. D., Ruseckas, A., and Samuel, I. D. W. Discrete Hopping Model of Exciton Transport in Disordered Media. *Phys. Rev. B* **2005**, *72*, 075206-075210.

(18) Gregg, B. A., Sprague, J. and Peterson, M. W. Long-Range Singlet Energy Transfer in Perylene Bis(phenethylimide) Films. *J. Phys. Chem. B* **1997**, *101*, 5362-5369.

(19) Donati, D.; Williams, J. O. Exciton Diffusion Lengths for Pure and Doped Anthracene Single-Crystals from Microscopic Measurements. *Mol. Cryst. Liq. Cryst.* **1978**, *44*, 23-32.

(20) Mulder, B. J. Anisotropy of Light Absorption and Exciton Diffusion in Anthracene Crystals Determined from Externally Sensitized Fluorescence. *Philips Res. Rep.* **1967**, *22*, 142-149.

(21) Simpson, O. Electronic Properties of Aromatic Hyrdocarbons. III. Diffusion of Excitons. *Proc. R. Soc. London* **1957**, *238*, 402-411.

(22) Lyons, B. P., and Monkman, A. P. The Role of Exciton Diffusion in Energy Transfer Between Polyfluorene and Tetraphenyl Porphyrin. *Phys. Rev. B* **2005**, *71*, 235201-235205.

(23) Wu, C. F., Zheng, Y. L., Szymanski, C., and McNeill, J. Energy Transfer in a Nanoscale Multichromophoric System: Fluorescent Dye-Doped Conjugated Polymer Nanoparticles. *J. Phys. Chem. C* **2008**, *112*, 1772-1781.

(24) Tousek, J.; Touskova, J.; Remes, Z.; Kousal, J.; Gevorgyan, S. A.; Krebs, F. C. Exciton Diffusion Length in Some Thermocleavable Polythiophenes by the Surface Photovoltage Method. *Synth. Met.* **2012**, *161*, 2727-2731.

(25) Jelly, E. E. Molecular, Nematic and Crystal States of I: I-Diethyl--Cyanine Chloride. *Nature (London)* **1936**, *139*, 631-632.

(26) Hayer, A., Van Regemorter, T., Höfer, B., Mak, C. S. K., Beljonne, D., and Köhler, A. On the Formation Mechanism for Electrically Generated Exciplexes in a Carbazole-Pyridine Copolymer. *J. Polym. Sci. Part B: Polym. Phys.* **2012**, *50*, 361-369.

(27) McNeill, J. D.; Barbara, P. F. NSOM Investigation of Carrier Generation, Recombination, and Drift in a Conjugated Polymer. *J. Phys. Chem. B* **2002**, *106*, 4632-4639.

(28) Hintschich, S. I.; Rothe, C.; Sinha, S.; Monkman, A. P.; de Freitas, P. S.; Scherf, U. Population and Decay of Keto States in Conjugated Polymers. *J. Chem. Phys.* **2003**, *119*, 12017-12022.

(29) Wu, C. F., Peng, H., Jiang, Y. and McNeill, J. Energy Transfer Mediated Fluorescence from Blended Conjugated Polymer Nanoparticles. *J. Phys. Chem. B* **2006**, *110*, 14148-14154.

(30) Hofmann, S.; Rosenow, T. C.; Gather, M. C.; Lussem, B.; Leo, K. Singlet Exciton Diffusion Length in Organic Light-Emitting Diodes. *Phys. Rev. B* **2012**, *85*, 245209-245216.

(31) Kelbauskas, L.; Bagdonas, S.; Dietel, W.; Rotomskis, R. Excitation Relaxation and Structure of TPPS4 J-Aggregates. *J. Lumin.* **2003**, *101*, 253-262.

(32) McNeill, J. D.; O'Connor, D. B.; Barbara, P. F. Imaging Organic Device Function with Near-Field Scanning Optical Microscopy. *J. Chem. Phys.* **2000**, *112*, 7811-7821.

(33) Adams, D. M.; Kerimo, J.; O'Connor, D. B.; Barbara, P. F. Spatial Imaging of Singlet Energy Migration in Perylene Bis(Phenethylimide) Thin Films. *J. Phys. Chem. A* **1999**, *103*, 10138-10143.

(34) Credo, G. M.; Carson, P. J.; Winn, D. L.; Buratto, S. K. Nanoscale Photophysics of Alq(3) Films. *Synth. Met.* **2001**, *121*, 1393-1394.

(35) Marciniak, H.; Teicher, M.; Scherf, U.; Trost, S.; Riedl, T.; Lehnhardt, M.; Rabe, T.; Kowalsky, W.; Lochbrunner, S. Photoexcitation Dynamics in Polyfluorene-Based Thin Films: Energy Transfer and Amplified Spontaneous Emission. *Phys. Rev. B* **2012**, *85*, 214204-214213.

(36) Bolinger, J. C.; Traub, M. C.; Adachi, T.; Barbara, P. F. Ultralong-Range Polaron-Induced Quenching of Excitons in Isolated Conjugated Polymers. *Science* **2011**, *331*, 565-567.

(37) Yu, J., Wu, C. F., Tian, Z. and McNeill, J. Tracking of Single Charge Carriers in a Conjugated Polymer Nanoparticle. *Nano Lett.* **2012**, *12*, 1300-1306.

(38) McNeill, J. D.; Kim, D. Y.; Yu, Z. H.; O'Connor, D. B.; Barbara, P. F. Near Field Spectroscopic Investigation of Fluorescence Quenching by Charge Carriers in Pentacene-Doped Tetracene. *J. Phys. Chem. B* **2004**, *108*, 11368-11374.

(39) Deussen, M.; Scheidler, M.; Bassler, H. Electric-Field-Induced Photoluminescence Quenching in Thin-Film Light-Emitting-Diodes Based on Poly(Phenyl-P-Phenylene Vinylene). *Synth. Met.* **1995**, *73*, 123-129.

(40) Szymanski, C., Wu, C. F., Hooper, J., Salazar, M. A., Perdomo, A., Dukes, A., and McNeill, J. Single Molecule Nanoparticles of the Conjugated Polymer MEH-PPV, Preparation and Characterization by Near-Field Scanning Optical Microscopy. *J. Phys. Chem. B* **2005**, *109*, 8543-8546.

(41) Lakowicz, J. R. *Principles of Fluorescence Spectroscopy*; Third ed.; Springer Science+Business Media, LLC: New York, 2006.

(42) Brouwer, A. M. Standards for Photoluminescence Quantum Yield Measurements in Solution (IUPAC Technical Report). *Pure Appl. Chem.* **2011**, *83*, 2213-2228.

(43) Seybold, G.; Wagenblast, G. New Perylene and Violanthrone Dyestuffs for Fluorescent Collectors. *Dyes Pigm.* **1989**, *11*, 303-317.

(44) Yang, Z.; Huck, W. T. S.; Clarke, S. M.; Tajbakhsh, A. R.; Terentjev, E. M. Shape-Memory Nanoparticles from Inherently Non-Spherical Polymer Colloids. *Nat. Mater.* **2005**, *4*, 486-490.

(45) Tian, Z., Yu, J., Wu, C. F., Szymanski, C. and McNeill, J. Amplified Energy Transfer in Conjugated Polymer Nanoparticle Tags and Sensors. *Nanoscale* **2010**, *2*, 1999-2011.

(46) Tian, Z. Y.; Yu, J. B.; Wang, X. L.; Groff, L. C.; Grimland, J. L.; McNeill, J. D. Conjugated Polymer Nanoparticles Incorporating Antifade Additives for Improved Brightness and Photostability. *J. Phys. Chem. B* **2013**, *117*, 4517-4520.

(47) Ntziachristos, V. Fluorescence Molecular Imaging. *Annu. Rev. Biomed. Eng.* **2006**, *8*, 1-33.

(48) Chen, R. Apparent Stretched-Exponential Luminescence Decay in Crystalline Solids. *J. Lumin.* **2003**, *102*, 510-518.

(49) Tvingstedt, K., Vandewal, K., Zhang, F., and Inganäs, O. On the Dissociation Efficiency of Charge Transfer Excitons and Frenkel Excitons in Organic Solar Cells: A Luminescence Quenching Study. *J. Phys. Chem. C* **2010**, *114*, 21824-21832.

(50) Simas, E. R., Gehlen, M. H., Pinto, M. F. S., Siquiera, J., and Misoguti, L. Intrachain Energy Migration to Weak Charge-Transfer State in Polyfluorene End-Capped with Naphthalimide Derivative. *J. Phys. Chem. A* **2010**, *114*, 12384-12390.

(51) Dykstra, T. E., Hennebicq, E., Beljonne, D., Gierschner, J., Claudio, G., Bittner, E. R., Knoester, J., and Scholes, G. D. Conformational Disorder and Ultrafast Exciton Relaxation in PPV-family Conjugated Polymers. *J. Phys. Chem. B* **2009**, *113*, 656-667.

(52) Kometani, N.; Nakajima, H.; Asami, K.; Yonezawa, Y.; Kajimoto, O. Luminescence Properties of the Mixed J-Aggregate of Two Kinds of Cyanine Dyes in Layer-by-Layer Alternate Assemblies. *J. Phys. Chem. B* **2000**, *104*, 9630-9637.

FIGURE CAPTIONS

Fig 1. (a) Structures of perylene red and PFBT. (b) Normalized perylene red absorbance (black line) and PFBT fluorescence (red line) in THF with spectral overlap region shaded. (c,d) Representative AFM image of undoped PFBT CPNs and particle size histogram.

Fig 2. (a) Fluorescence spectra of perylene red doped PFBT CPNs at various doping ratios. (b) Stern-Volmer quenching plot. (c) Total fluorescence quantum yield vs. quencher-donor molecular ratio.

Fig 3. (a) Normalized fluorescence lifetime decay traces for PFBT in THF and doped CPNs. (b) Single exponential (blue), bi-exponential weighted average (green), and KWW (red) lifetimes of perylene red doped CPNs. Inset: KWW heterogeneity parameter *ß* vs. perylene red dopant percent.

Fig. 4. Comparison of simulated (blue) and experimental (black) (a) quenching efficiency, (b) average lifetime, and KWW stretch parameter *ß* (inset) vs. quencher/donor molecular ratio.

FIGURES

Figure 1

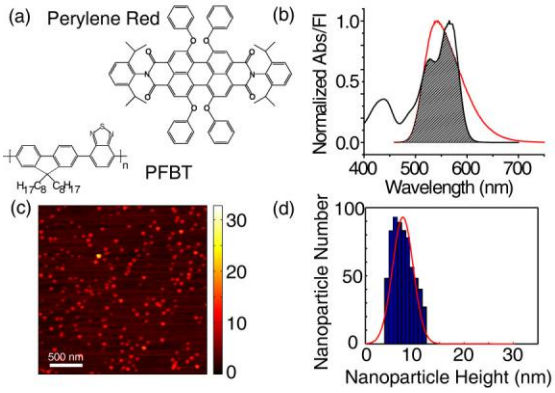

Figure 2

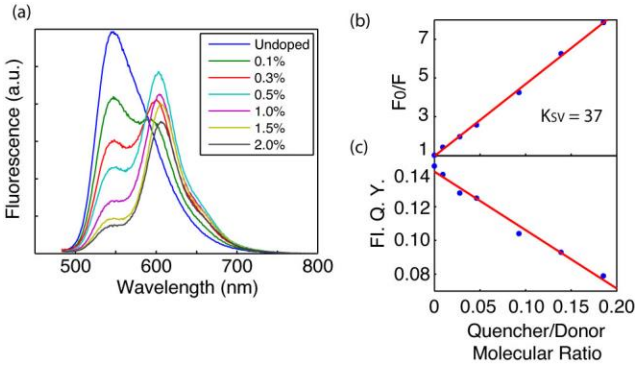

Figure 3

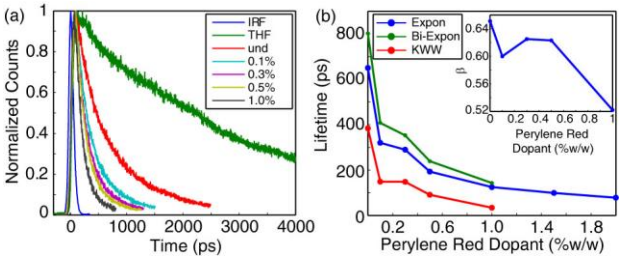

Figure 4

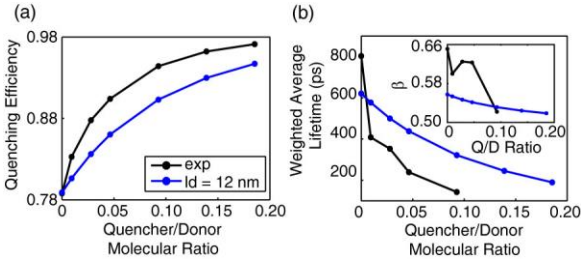

TOC Figure